Cell, Vol. 108, 283–295, January 25, 2002, Copyright ©2002 by Cell Press

Structure of the Reovirus Membrane-Penetration Protein, μ1, in a Complex with Its Protector Protein, σ3

Susanne Liemann,[1] Kartik Chandran,[2] Timothy S. Baker,[3] Max L. Nibert,[2] and Stephen C. Harrison[1,4]

[1]Howard Hughes Medical Institute
Children's Hospital
Harvard Medical School
320 Longwood Avenue
Boston, Massachusetts 02115

[2]Department of Microbiology and Molecular Genetics
Harvard Medical School
Boston, Massachusetts 02115

[3]Department of Biological Sciences
Purdue University
West Lafayette, Indiana 47907

Summary

Cell entry by nonenveloped animal viruses requires membrane penetration without membrane fusion. The reovirus penetration agent is the outer-capsid protein, μ1. The structure of μ1, complexed with its "protector" protein, σ3, and the fit of this $\mu1_3\sigma3_3$ heterohexameric complex into the cryoEM image of an intact virion, reveal molecular events essential for viral penetration. Autolytic cleavage divides μ1 into myristoylated μ1N and μ1C. A long hydrophobic pocket can receive the myristoyl group. Dissociation of μ1N, linked to a major conformational change of the entire μ1 trimer, must precede myristoyl-group insertion into the cellular membrane. A myristoyl switch, coupling exposure of the fatty acid chain, autolytic cleavage of μ1N, and long-range molecular rearrangement of μ1C, thus appears to be part of the penetration mechanism.

Introduction

Nonenveloped viruses of eukaryotes must enter cells by penetrating the lipid bilayer of a cellular membrane, without having a viral membrane of their own to fuse with it (Harrison, 2001). The mechanism of this penetration remains a significant puzzle. In the case of reoviruses, the viral core, an icosahedral structure about 700 Å in diameter (Dryden et al., 1993), enters the cytoplasm, where it functions intact as a transcriptional complex (Borsa et al., 1981; Shatkin and LaFiandra, 1972). Entry, thus, appears to require significant perforation of the membrane through which the core penetrates. The process might involve specific pore formation, a less defined, local disruption of the bilayer, or even a transiently enveloped intermediate.

Reoviruses have a segmented, dsRNA genome, encapsidated in the viral core, which is in turn surrounded by an outer protein coat (Figure 1A) (Nibert and Schiff, 2001). The major core protein, known as λ1, forms an icosahedral shell, stabilized by surface binding of a second core protein, σ2 (Reinisch et al., 2000). Twelve turret-like pentamers of a third core protein, λ2, also project from this shell (Dryden et al., 1993; Reinisch et al., 2000). RNA transcripts, produced by the viral polymerase complexes (λ3 and μ2) inside the shell, exit through the λ2 turrets, which cap the 5′ ends. In the virion, the cores are coated in equimolar ratio by a layer of the two proteins studied here, μ1 and σ3. These proteins form a T = 13*l* icosahedral lattice, interrupted at the 5-fold axes by the λ2 turrets (Dryden et al., 1993). A trimer of one further protein, σ1, associates with each turret (Furlong et al., 1988).

Like most animal viruses, reoviruses are activated for infection by proteolytic cleavages. Exposure of virions to proteases in the intestinal lumen (reoviruses infect intestinal cells) or in endocytic vacuoles leads to formation of "infectious subviral particles" (ISVPs) (Chang and Zweerink, 1971; Silverstein et al., 1970). These particles lack σ3, and their σ1 proteins have undergone a conformational change that results in fiber-like spikes projecting from each 5-fold vertex (Dryden et al., 1993). Moreover, at some time between assembly and activation, μ1 undergoes a cleavage, believed to be autolytic, into a small, N-terminal fragment (μ1N, 4 kDa) and a large, C-terminal fragment (μ1C, 72 kDa) (Nibert et al., 1991). This cleavage depends on the presence of σ3, on the N-terminal, myristoyl group of μ1, and on the μ1 residues 42 and 43 (Asn-Pro) at the cleavage site (Tillotson and Shatkin, 1992).

The first step in reovirus entry is σ1 attachment to cell surface receptors (Lee et al., 1981). The fiber-like conformation of σ1 in the ISVP may facilitate receptor binding. When infection is carried out with cells in culture, however, unmodified virions can attach, and endosomal proteases then strip off σ3. μ1, exposed by σ3 removal, provides the membrane penetration machinery. Indeed, when cell association is enhanced by high concentration, σ1 is dispensable, and cores recoated with recombinant μ1 and σ3 can enter and infect (Chandran et al., 1999). ISVPs generated in vitro, but not intact virions or cores, induce release of ^{51}Cr from preloaded mouse L cells (Borsa et al., 1979; Lucia-Jandris et al., 1993), release of hemoglobin from erythrocytes (Chandran and Nibert, 1998), and opening of current-conducting pores in planar lipid bilayers (Tosteson et al., 1993). Each of these effects is interpreted to indicate some sort of perforation of the target membrane. Monoclonal antibodies directed against μ1 inhibit ^{51}Cr release by interfering with a postattachment step (Hooper and Fields, 1996a), and ethanol-resistant mutants, which have point mutations in μ1, show a strong correlation between ethanol sensitivity and the capacity to cause ^{51}Cr release (Hooper and Fields, 1996b).

The μ1 protein (76 kDa) binds the σ3 protein (41 kDa) in solution, and equal copy numbers of the trimeric μ1 and the finger-shaped σ3 are closely associated on the virion outer capsid (Dryden et al., 1993). The μ1-σ3 asso-

[4]Correspondence: harrison@crystal.harvard.edu

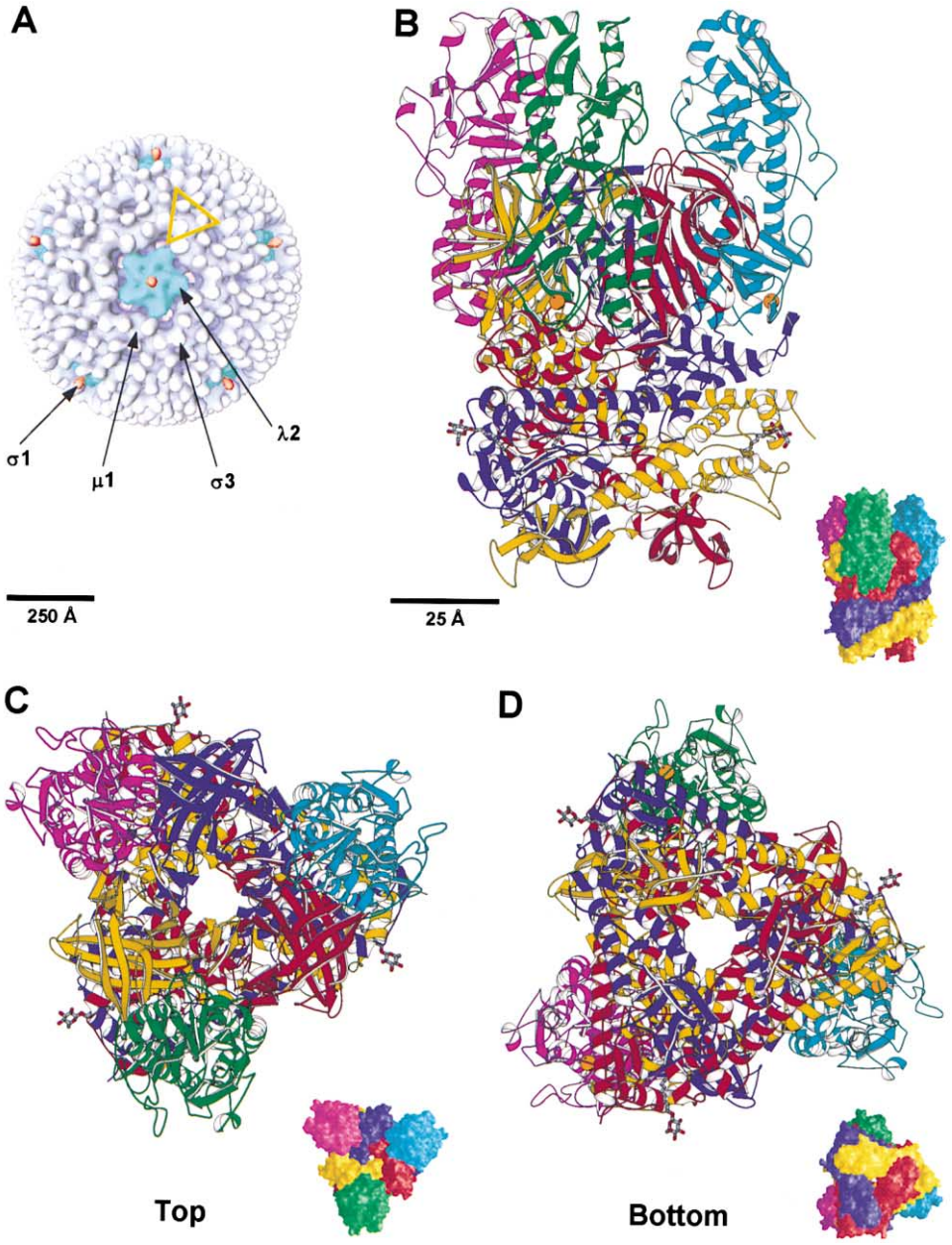

Figure 1. Structure of the $\mu1_3\sigma3_3$ Heterohexamer

(A) Surface of a reovirus particle (Dryden et al., 1993), with an example of each of the four exposed proteins labeled. The yellow triangle outlines one $\mu1_3\sigma3_3$ complex.

(B) A $\mu1_3\sigma3_3$ complex, viewed from the side. The bottom of the complex would contact $\sigma2$ proteins on the surface of the reovirus core. Three $\sigma3$'s (41 kDa; shown in green, cyan, and magenta) bind to the upper part of the underlying trimer of $\mu1$ trimer (76 kDa; shown in red, blue, and yellow). The three $\mu1$ chains are wound tightly around each other. Each $\sigma3$ contacts two $\mu1$'s.

(C) View from the top after a 90° rotation of the model in (B) around a horizontal axis within the plane of the paper.

(D) View from the bottom. Insets: Molecular surfaces of the $\mu1_3\sigma3_3$ complex showing $\mu1$ and $\sigma3$ in the same color code.

ciation is essential for assembly of outer capsids around progeny cores (Fields et al., 1971; Shing and Coombs, 1996), and recombinant $\mu1_3\sigma3_3$ complexes recoat virion-derived cores in vitro (Chandran et al., 1999). In addition to serving as a "protector" for $\mu1$, $\sigma3$ has a regulatory function during infection: it binds dsRNA (Huismans and Joklik, 1976; Schiff et al., 1988), thereby preventing activation of the interferon-induced inhibitory protein kinase (PKR) (Imani and Jacobs, 1988; Sharpe and Fields, 1982). The dsRNA binding capacity is eliminated upon association with $\mu1$ (Tillotson and Shatkin, 1992). The crystal structure of $\sigma3$ alone shows it to be an elongated molecule, with a strong dimer contact (Olland et al., 2001). The dimer appears to be the prevalent form in solution, and it may be the form that binds dsRNA (Olland et al., 2001). The dimer contacts must be broken when $\sigma3$ associates with $\mu1$.

We describe here the structure, determined at 2.8 Å

resolution, of a heterohexameric complex, $\mu1_3\sigma3_3$, from human reovirus type 1 Lang (T1L). The $\mu1$ chains in the crystals have been cleaved autolytically into $\mu1N$ and $\mu1C$. The myristoylated $\mu1N$ fragments are tightly integrated into the folded structure, such that a significant conformational rearrangement, a large-scale "myristoyl switch," is required to release them. Atomic coordinates for 200 copies of the $\mu1_3\sigma3_3$ heterohexamer can be positioned in an 18 Å resolution density map of the virion, derived from electron cryomicroscopy. Inclusion of the crystallographically determined structure of the reovirus core (Reinisch et al., 2000) generates a quasi-atomic model for a 100 MDa assembly—the entire icosahedrally ordered part of a virion. The ensemble of structural observations leads to a model for how the nonenveloped reovirus particle initiates penetration of the endosomal or plasma membrane of the host cell during infection.

Results and Discussion

Preparation, Crystallization, and Structure Determination

The complex of $\mu1$ and $\sigma3$ was obtained by coexpression of the two proteins in Sf21 insect cells infected with a recombinant baculovirus (Chandran et al., 1999) and was purified as described in Experimental Procedures. Analytical ultracentrifugation revealed the molecular mass of the complex to be about 350 kDa (data not shown), corresponding to a "heterohexamer," $\mu1_3\sigma3_3$. Crystals of the complex were obtained only with the addition of alkyl sugar detergents such as n-octyl-β-D-glucopyranoside (β-octyl glucoside) to the crystallization drop. The structure was determined by a combination of multiple isomorphous replacement and anomalous scattering, using a mercury (Hg) and a selenomethionine (SeMet) derivative and 3-fold noncrystallographic symmetry (NCS) averaging. The current model of the heterohexamer was refined at a resolution of 2.8 Å. It contains three copies of the full-length (residues 1–365), N terminally acetylated $\sigma3$ and three copies of $\mu1$, residues 10–71, and 97–675. The coordinates have been submitted to the PDB (accession number 1JMU).

Overall Molecular Architecture

Three monomeric $\sigma3$ "fingers" project from a trimeric $\mu1$ base (Figure 1). Each $\sigma3$ contacts two $\mu1$ subunits within each trimer. The overall dimensions of the complex are approximately 130 Å × 100 Å × 95 Å. $\sigma3$ has an α/β structure with two lobes organized around a long, central α helix (Olland et al., 2001). The large lobe faces the virion surface; the small lobe contains the structural zinc-binding motif and mediates most contacts to $\mu1$. The structure of $\sigma3$ in complex with $\mu1$ is essentially identical to that of a monomer of free $\sigma3$ (Olland et al., 2001), with an rms deviation of only 0.62 Å for all Cα atoms.

The $\mu1$ trimer at the base of the complex has a compact, triangular architecture with overall dimensions of 100 Å × 80 Å × 70 Å. The three $\mu1$ molecules are coiled around each other with a right-handed twist. Each subunit traverses about 360° as it winds from bottom to top (Figure 2A). At the center of the trimer is a hydrophilic pore. A $\mu1$ subunit presents about 5200 Å^2 of buried surface to each of its neighbors in the trimer; thus, about 33% of its total area contributes to trimer stability. Extended loops beneath the $\mu1$ trimer allow variable contacts between the T = 13*l* icosahedral lattice of the $\mu1$ shell and proteins of the reovirus core. In the crystals, the $\mu1$ polypeptide chain has been cleaved into $\mu1N$ and $\mu1C$ fragments (Nibert et al., 1991). The N-terminal myristoyl group of $\mu1$ attached to Gly2, present in the recombinant $\mu1$ used for crystallization as verified by MALDI-TOF mass spectrometry of the N terminally blocked $\mu1N$ (data not shown), is disordered in the electron density together with residues 2–9. Instead, we find a well-ordered β-octyl glucoside molecule tucked into a long hydrophobic pocket in $\mu1$, close to the first ordered N-terminal residue, Thr10. The C-terminal 33 residues of $\mu1$ (676–708) are also disordered in the crystal. On the virion surface, they are in proper position to interact with C-terminal tails from adjacent trimers (see section "Fit of the $\mu1_3\sigma3_3$ molecular model into the low-resolution structure of a virion," below)

The μ1 Subunit

The $\mu1$ polypeptide chain folds into four distinct domains (Figure 2): three predominantly α-helical domains, which constitute the lower part of the $\mu1$ trimer (domains I, II, and III), and a jelly-roll β-barrel, which forms the outward-facing "head" (domain IV). Comparison, using the DALI algorithm (Holm and Sander, 1993), of domains I–III with all three-dimensional protein structures in the Protein Data Bank reveals no closely related protein fold.

Domain I: The basal domain I includes residues 30–186. Residues 72–96 are disordered in the electron density and probably form a flexible loop facing toward the core. Residues 51–60 on the surface of the trimer that faces the core also have large thermal parameters ($B > 100$ Å^2) consistent with flexibility. Contacts with the core must be different for each of the ten icosahedrally distinct $\mu1$ subunits, and some flexibility in this part of the molecule is thus clearly essential. Domain I is an α/β structure, with a short, twisted, five-stranded, antiparallel β sheet at the very base of the $\mu1$ trimer (β2–β6) and two nearly parallel α helices (αA and αB) (Figure 3). Helix B extends with a slight kink into domain II (αB′). The conserved autolytic cleavage site C-terminal to residue 42 (Nibert et al., 1991) lies in a pocket on the upper surface of domain I.

Domain II: Domain II is the central structure of the $\mu1$ base. It contains 145 residues in three discontinuous segments of the $\mu1$ polypeptide chain (Figures 2 and 3). One of these segments (residues 2–29) is the first part of $\mu1N$. Residues 2–9 and the myristoyl group are disordered in the crystal structure, probably because a β-octyl glucoside has displaced the fatty-acyl chain from its pocket. Residues 19 and 21 make a short β strand, which tethers $\mu1N$ firmly to the rest of the domain. The second segment in domain II (residues 187–278) folds into a compact cluster of three α helices, which form the presumptive myristoyl pocket. The C-terminal segment, residues 643–672, terminates in a long α helix (αK), oriented almost parallel to the trimer base. The last well-defined residue, Pro675, lies about halfway up the lateral face of the $\mu1$ trimer, defining a sharply triangular cross section. The C-terminal tails (residues 676–708) emerge disordered from each of the corners of this triangle.

Domain III: This mainly α-helical domain contains 125

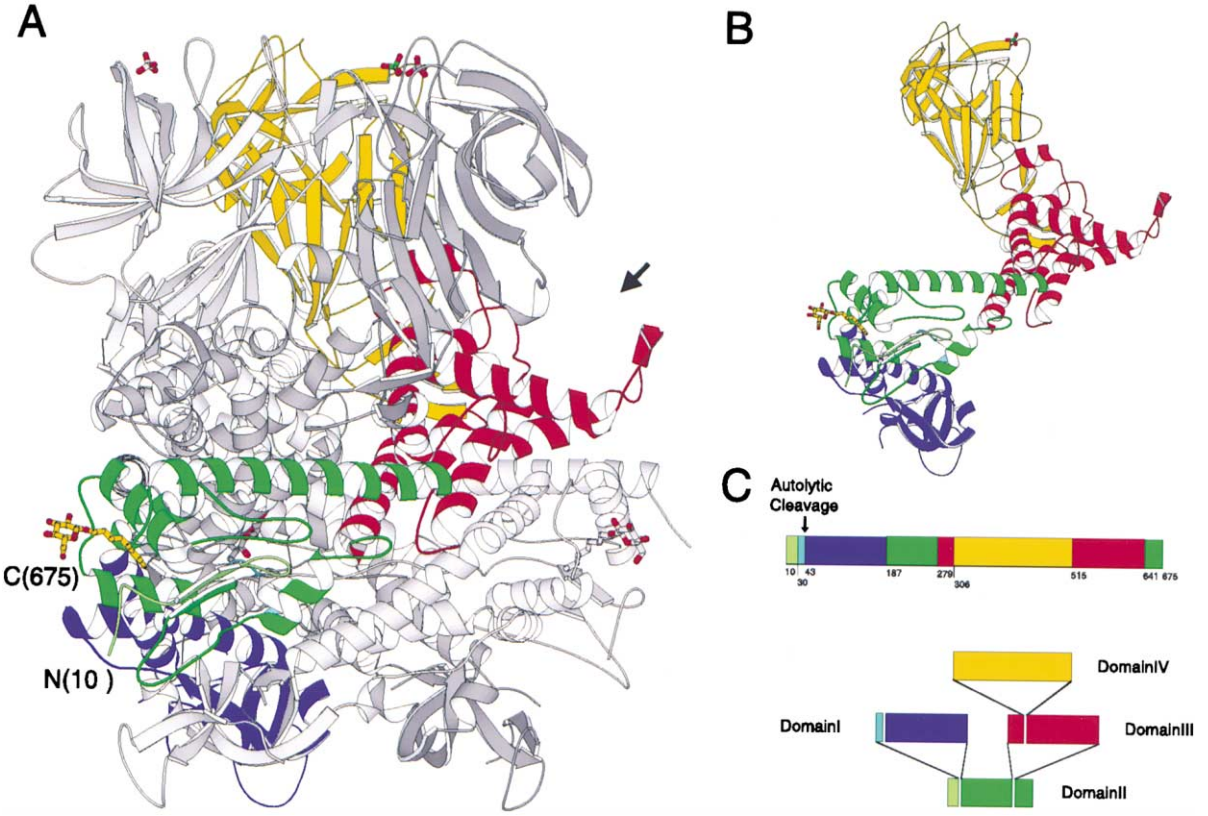

D

```
mul T1L MGNASSIVQTINVTGDGNVFKPSAETSSTAVPSLSLSPGMLNPGGVPWIAIGDETSVTSP
mul T2J ..........................................................I.........
mul T3D ..........................................................I.........
VP5 GCR .W.VQTS.N.Y.I.....S.T.TSDMT...A.AID.K..V...T.KL.RP..TSVATIDS
          10        20        30        40        50        60

mul T1L GALRRMTSKDIPETAIINTDNSSGAVPSESALVPYNDEPLVVVTEHAIANFTKAEMALEF
mul T2J ..........................................................I.........
mul T3D ..................................I.............T.................
VP5 GCR ----------------------------L.I.SDRFGQYSF.N.GMRET.S..LFDINM
          70        80        90        100       110       120

mul T1L NREFLDKLRVLSVSPKYSDLLTYVDCYVGVSARQALNNFQKQVPVITPTRQTMYVDSIQA
mul T2J ..........................................................I.........
mul T3D .......M..................................................I.........
VP5 GCR WQPLFQATKTGCGPIVL.SFT.TTSG...AT.GD..D.PVTNGVF.STVQIMNLQRT.A.
          130       140       150       160       170       180

mul T1L ALKALEKWEIDLRVAQTLLPTNVPIGEVSCPMQSVVKLLDDQLPDDSLIRRYPKEAAVAL
mul T2J ..........................................................I.........
mul T3D ..........................................................I.........
VP5 GCR RMRDVAL.QKH.DT.M.M.TPDISA.SA..NWK.LLAFAK.I..L.N.CLT..N.FYNVA
          190       200       210       220       230       240

mul T1L AKRNGGIQ--WMDVSEGTVMNEAVNAVAASALAPSASAPPLEEKSKLTEQAMDLVTAAEP
mul T2J ........--..................................................--.....
mul T3D ........--..................................................--.....
VP5 GCR IH.YPALK..NP.TKLPDAQAHPLGE..GAFN.ATSEVGS.VGS.STLS..ISTMAGKDL
                  250       260       270       280       290

mul T1L EIIASLVPVPAPVFAIPPKPADYNVRTLKIDEATWLRMIPKTMGTPFQIQVTDNTGTNWH
mul T2J ..........................................................T.........
mul T3D .....A..................R..........................N..
VP5 GCR DL.EADT.L.VS..TPSLA.RS.RPAFI.PED.K.IAEFNN.S---LIRKTLTYS.ATYT
          300       310       320       330       340       350

mul T1L LNLRGG-TRVVNLDQIAPMRFVLDLGGKSY-KETSWDPNGKKVGFIVFQSKIPFELWTAA
mul T2J ......-..........................-..........................
mul T3D L.....-..........................-..........................
VP5 GCR VQ.GP.....IDMNAMIDSVLT..VS.TIL.YD..P.LSTSVPA.VLI.TSV.IQQV.T.
          360       370       380       390       400       410

mul T1L SQIGQATVVNYVQLYAEDSSFTAQSIIATTSLAYNYEPEQLNKTDPEMNYYLLATFIDSA
mul T2J ..........................................................A.....
mul T3D ..........................................................I.....
VP5 GCR AN.TAI...SAAGAS.INLAINVRGQPRFNM.HLQATF.RETI.G-IPYI.G.G..LIPS
          420       430       440       450       460       470

mul T1L AITPTNMTQPDVWDALLTMSPLSAGEVTVKGAVVSEVVPAELIGSYTPESLNASLPNDAA
mul T2J ..........................................I.......................
mul T3D ..TPT.....................................I.......................
VP5 GCR PT.S..FSN.TLM.G...VT.VLLR.T.Y..E..DAI...TVMANQ.S.EVASA.A...I
          480       490       500       510       520       530

mul T1L RCMIDRASKIAEAIKIDDDAGPDEYSPNSVPIQGQLAISQLETGYGVRIFNP--KGILSK
mul T2J ..........................................................--.....
mul T3D ..........................................................--.....
VP5 GCR VLVSNHLN.L.NVVGDAIPVASKTDDSATSA.VSR..VQHKLSQV.QASPT...YPL.WR
          540       550       560       570       580       590

mul T1L IASRAMQAFIGDPSTIITQAAPVLSDKNNWIALAQGVKTSLRTKSLSAGVKTAVSKLSSS
mul T2J ..........................................................
mul T3D ..........................................................
VP5 GCR R.K..ASM.VSN..LALQVGI...TQSGMLS..TS..G.A...G..GK..TD.SE..RAR
          600       610       620       630       640       650

mul T1L ESIQNWTQGFLDKVSTHFPAPKPDCPTNGDGSEPSARRVKRDSYAGVVKRGYTR
mul T2J ..........................................................
mul T3D ....N.........A.........T.....ES.N..V..............
VP5 GCR Q.LTVAK.A.F.QIGNLW.GK----------------------------------
          660       670       680       690       700
```

residues in two discontinuous polypeptide-chain segments (279–305 and 515–640). There are five α helices (αF–αJ) and a short β strand (β25). Helices F, G, and J are an antiparallel bundle linking domains II and IV. Helices H and I and the exposed bridge between them project laterally, forming a cradle for the base of σ3. The exposed bridge contains the δ/ϕ cleavage sites C-terminal to residue 581 (cleavage with chymotrypsin) and 584 (cleavage with trypsin) (Nibert and Fields, 1992).

Domain IV: The head domain at the tip of the μ1 trimer (residues 306–514) is a jelly-roll β barrel, similar in fold to those found in numerous other viral proteins (Harrison, 2001). There are two antiparallel β sheets, one with four and one with five β strands. The μ1 jelly roll has three additional β hairpin insertions, which participate in μ1-σ3 or μ1-μ1 interactions within the heterohexamer (Figure 3). The long β11/β12 hairpin flanks the five-stranded β sheet on the $\mu1_3\sigma3_3$ surface and interacts with the large and small lobes, respectively, of two different σ3 molecules. This β-hairpin also contains a site that binds a very well-ordered sulfate ion at the apex of the μ1 subunit. The β17/β18 hairpin contacts another μ1 molecule around the upper opening of the central channel. Phe437 constricts the mouth of this otherwise hydrophilic channel to a diameter of 5 Å. The β22/β23 hairpin interacts with the small lobe of a σ3 subunit.

The σ3 Subunit and the μ1/σ3 Interface

Each σ3 contacts two μ1 subunits. The smaller, zinc binding lobe of σ3 rests between two μ1 jelly-roll domains and buries a total of 1685 Å^2 in the contact. Thus, σ3 appears to lock the μ1 head domains in place, consistent with the observation that coexpression of σ3 is required for μ1 folding and trimerization (Chandran et al., 1999). The projecting loop that joins αH and αI in μ1 domain III (Figure 3), supports the base of σ3, and μ1 residues 581–583 (β25) anchor σ3 residues 69–71 in a small β sheet. This β strand in σ3 is the only secondary structure element not seen in the σ3 dimer structure (Olland et al., 2001). The αH-αI loops of μ1 become protease sensitive when σ3 is lost (Nibert and Fields, 1992). There is significant overlap of the σ3 residues that contact μ1 in the complex with those that stabilize the σ3 dimer (Olland et al., 2001). Formation of a $\mu1_3\sigma3_3$ complex will therefore compete with σ3 dimerization, and σ3 dimers may be disrupted at a sufficient μ1 concentration in favor of the heterohexamer. The dimer is proposed to be important for dsRNA binding by σ3 (Olland et al., 2001), and this competition may be part of the mechanism whereby μ1 counteracts the effects of σ3 on PKR activation and translation (Tillotson and Shatkin, 1992).

The Autolytic Cleavage Site

The μ1 subunits in the crystals have clearly undergone cleavage into μ1N and μ1C: the Cα atoms of residues 42 and 43 are separated by about 9 Å. The recombinant complex, however, prepared for crystallization and treated with β-octyl glucoside, contained largely uncleaved μ1, as determined by SDS-PAGE of samples that were not heated to boiling prior to electrophoresis (data not shown). We have not yet determined what has triggered the autocleavage reaction during crystallization. It is possible that small conformational shifts at the surface of the complex accompany the peptide bond cleavage and correlate with stable crystal contacts, leading to selective incorporation of cleaved complexes. The site of cleavage faces the hydrophilic channel at the center of the trimer, but the small diameter of the channel prevents access to the cleavage site by exogenous protease, consistent with an autolytic mechanism. σ3 is unlikely to have contributed directly to cleavage, because it is not in contact with the region around the scissile bond. Several residues in the vicinity of the scissile bond are candidate participants in the reaction (Figure 4). Of these, Thr 104, Glu 105, and His 106 are all on helix A of the same subunit, and Lys 113 is on helix A of an adjacent μ1. Glu 105 and Lys 113 are linked by a salt bridge. While all four residues are conserved in mammalian reoviruses, Thr 104 and His 106 are not conserved in grass carp hemorrhagic virus VP5 (GenBank AF239175), the aquareovirus homolog of μ1. We suggest that the likely nucleophile is Asn 42 itself and that the mechanism resembles one discovered recently for a similar autolytic cleavage in nodaviruses (J. Johnson, personal communication). The stage at which virion-associated μ1 is normally cleaved has not been determined with certainty. If the purified $\mu1_3\sigma3_3$ heterohexamer is prepared for SDS-PAGE by boiling the sample, we observe almost complete cleavage of μ1. The same sample, prepared without boiling, contains largely intact μ1. Elevated temperature during denaturation appears to promote autolysis. Because most experiments using SDS-PAGE are carried out with boiled samples, published studies of the timing of μ1 autolysis may have been subject to this source of artifact (Nibert et al., 1991;

Figure 2. The μ1 Protein

(A) The μ1 trimer shown without bound σ3. One μ1 subunit is colored by domain (domain I, light and dark blue [μ1N, μ1C]; domain II, light and dark green [μ1N, μ1C]; domain III, red; domain IV, yellow); the two other μ1 subunits are in gray. The β-octyl glucoside in the colored subunit is in yellow; the sulfate ion in green and red. The σ3 binding site is indicated by an arrow.

(B) Ribbon diagram of an isolated μ1 subunit (coloring as in [A]).

(C) Domain segmentation of the amino acid sequence as determined from the three-dimensional structure. Domain color code as in (A). The central domain II contains domains I and III as "inserts," and domain III similarly contains domain IV.

(D) Amino acid sequence alignment of reovirus μ1 proteins. One representative of each of the three major human serotypes is shown: μ1 T1L (Chandran et al., 1999), μ1 T2J (Wiener and Joklik, 1988), and μ1 T3D (Jayasuriya et al., 1988). Also shown is the sequence of VP5 of grass carp hemorrhagic virus (GenBank accession number AAG17823), an aquareovirus outer capsid protein with 29% sequence identity to μ1 T1L. Amino acid numbering as in the μ1 T1L sequence. Secondary structure elements, derived from the coordinates using the program DSSP (Kabsch and Sander, 1983), are presented as tubes for α helices and arrows for β strands. The segments of the four domains are shown in the same color code as in (A). The arrowhead just before p2 shows the position of the autolytic cleavage. Dots indicate amino acid identities; dashes show gaps.

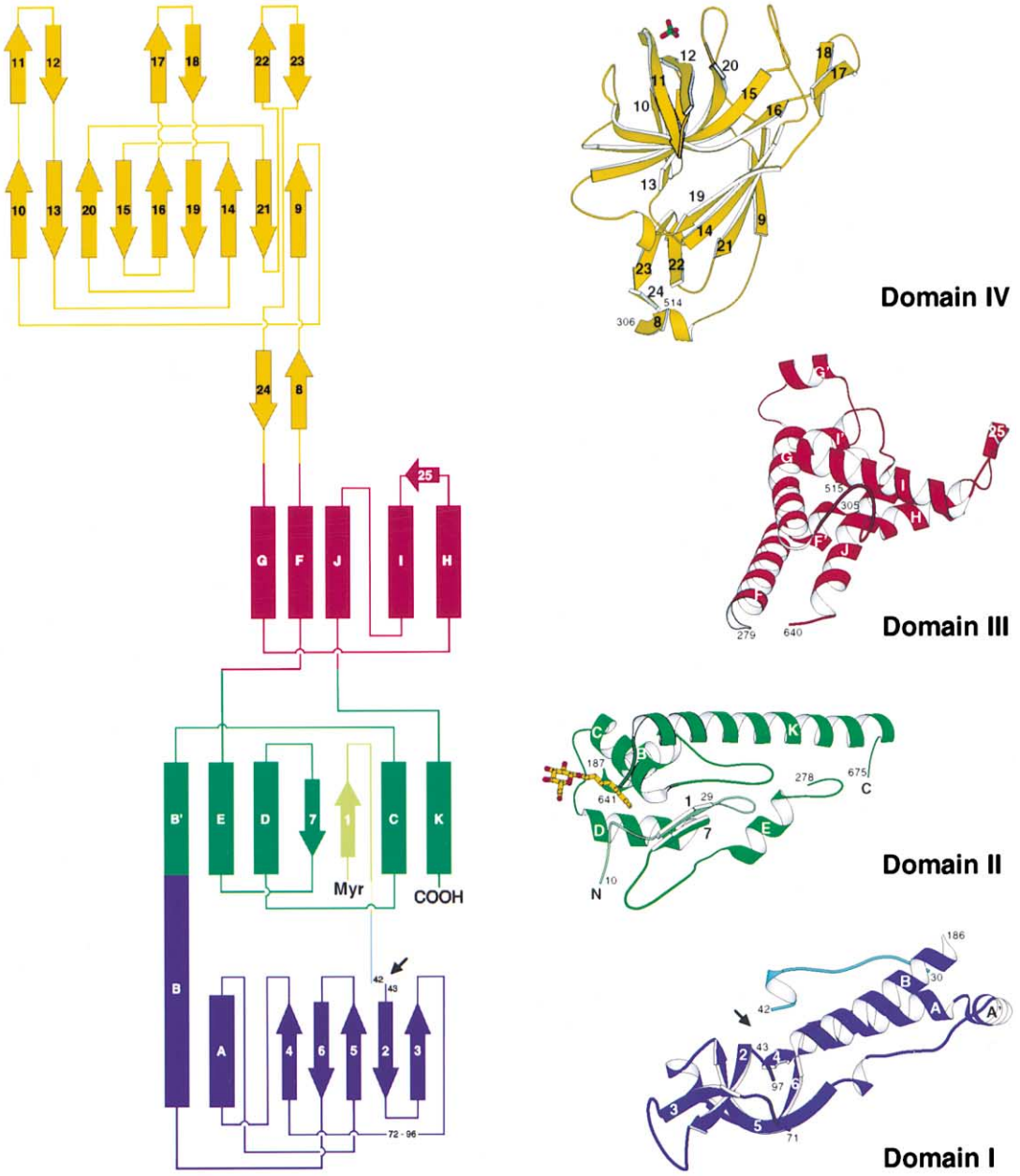

Figure 3. Fold of the μ1 Monomer

Left: Folding diagram of the μ1 polypeptide chain. α helices are shown as rectangles, β strands as arrows. Right: Ribbon representations of the four individual domains. The view for domains II and III is the same as for the colored μ1 monomer in Figure 2A; the view for domains I and IV is the same as for the yellow μ1 monomer in Figure 1B. The color code for the four domains is the same as in Figure 2. The β-octyl glucoside molecule bound to domain II is in yellow; the sulfate ion bound to domain IV, in green and red. The arrow shows the position of autolytic cleavage in domain I.

Zweerink and Joklik, 1970). Cleavage of μ1 might occur either during viral assembly, triggered by contacts of μ1 with proteins of the reovirus core and adjacent μ1 trimers, or during viral entry, when conformational rearrangements probably expose the μ1 N-terminal myristoyl groups for direct interaction with the host cell membrane. The myristoyl pockets and the scissile bonds are at about the same radial positions in the virion or ISVP. About 25 Å separates each myristoyl pocket at the margin of the heterohexamer from the nearest μ1N/μ1C cleavage point, which belongs to the clockwise-related neighbor. It is therefore possible that autolysis and myristoyl group exposure are coupled events.

Alkyl-Chain Binding Site

A β-octyl glucoside molecule tucked into a long hydrophobic pocket of μ1 was detected in a 3-fold averaged $F_o - F_c$ difference map. The exposed head group of the detergent molecule is close to amino acid Thr10, the first well-ordered residue of μ1. We propose that

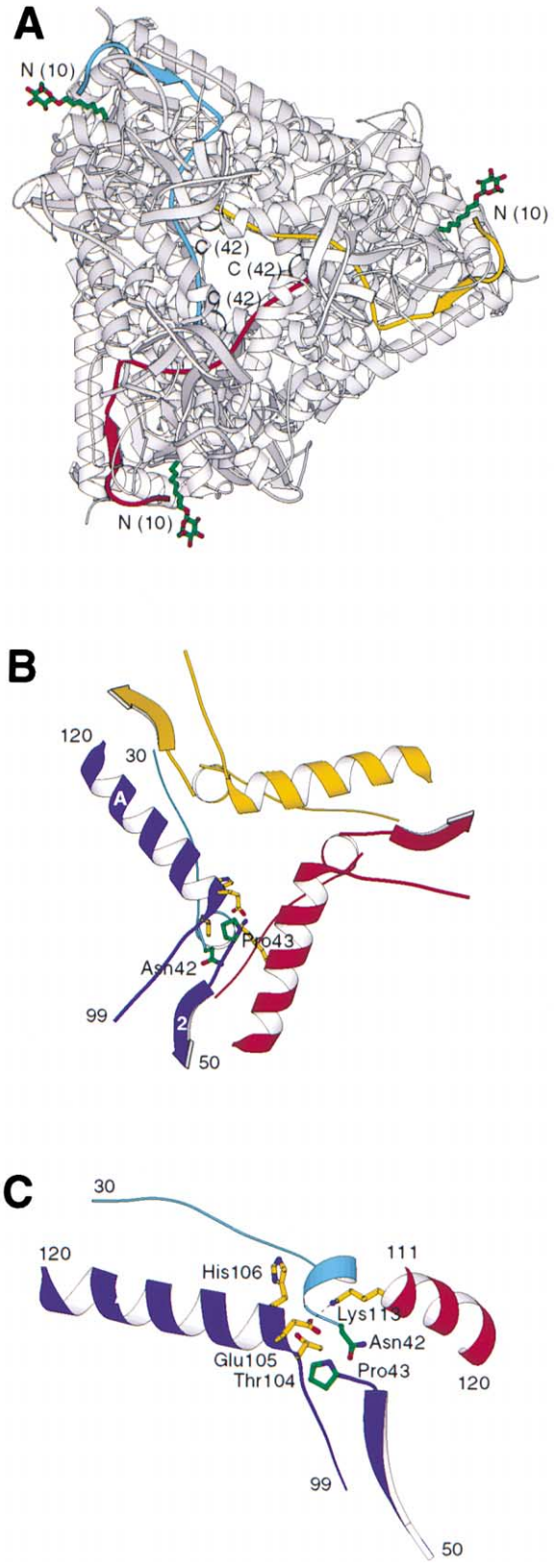

Figure 4. Autolytic Cleavage Site in μ1

(A) μ1 trimer viewed from the bottom. The three μ1N peptides are in light blue, yellow, and red; all three μ1C are in gray. The three β-octyl glucoside molecules are in green. The first ordered residue at the N terminus, Thr10, is indicated with "N."

(B) Close up of the three μ1N peptides with the adjacent helices A of the three μ1C chains. For the blue μ1 molecule, μ1N is shown in light blue, μ1C in dark blue, side chains of Asn42 and Pro43 in green, and side chains of Thr104, Glu105, His106, and Lys113 in close vicinity to the cleavage site in yellow.

(C) The cleaved μ1 polypeptide chain as seen from the side. The intermolecular salt bridge Glu105/Lys113 is indicated.

this pocket normally sequesters the N-terminal myristoyl group of μ1. The displaced myristoyl group is disordered in the crystals, along with residues 2–9. The myristoyl moiety could be shielded in a detergent micelle beneath the $\mu1_3\sigma3_3$ heterohexamer; the layer-like crystal packing can accommodate a detergent micelle in this location. The alkyl part of the bound β-octyl glucoside inserts into a hydrophobic pocket in domain II of μ1, framed by helices B′, C, and D and flanked by a short antiparallel β sheet of strands 1 and 7 (Figure 5A). Side chains from nearly 20 residues contribute to this hydrophobic pocket. All of these residues are conserved in the μ1 proteins of different mammalian orthoreovirus isolates (Figure 2C). The hydrophobic cleft completely engulfs the alkyl chain of the β-octyl glucoside, and the pocket appears deep enough to accommodate the six additional methylenes of a myristoyl chain.

Anion Binding Site

A sulfate ion, probably derived from the crystallization buffer, is bound at a site in domain IV. The anion would lie on the outermost, solvent-exposed surface of an ISVP (Figure 5B). Five main-chain amides (residues 340–343 and 363) coordinate the anion. The coordination resembles the binding of phosphates by loops in nucleotide binding proteins and protein kinases (Bossemeyer, 1994; Saraste et al., 1990). Although the sequence at this site is not highly conserved in homologous proteins (Figure 2C), we suggest below that it may bind phospholipid headgroups during reovirus infection.

Fit of the $\mu1_3\sigma3_3$ Molecular Model into the Low-Resolution Structure of a Virion

The surface of the virion contains 200 $\mu1_3\sigma3_3$ heterohexamers, at positions of 3-fold symmetry (local and strict) in a T = 13*l* icosahedral lattice. We inserted the $\mu1_3\sigma3_3$ structure into an 18 Å resolution three-dimensional image reconstruction of a T1L virion. There is a good fit for all four icosahedrally distinct heterohexamers (Figure 6), indicating that no large-scale rearrangements occur when the complex assembles onto the surface of a core. Close contacts of μ1 and σ3 subunits in 2-fold-related complexes stabilize the assembly. The σ3/σ3 and σ3/μ1 contacts are relatively limited, but μ1/μ1 interactions are extensive (Figure 6). The latter will persist in the ISVP. Contacts with the core involve σ2 and λ2; the fit shows no interaction with λ1. Interactions with the pentameric λ2 turrets involve many of the same σ3 and μ1 residues that participate in contacts with other heterohexamers; on λ2, all three enzymatic domains and the scaffold domain contribute, but the outward-facing, C-terminal flap does not (Reinisch et al., 2000). The three-dimensional image reconstruction of the virion has a "blob"

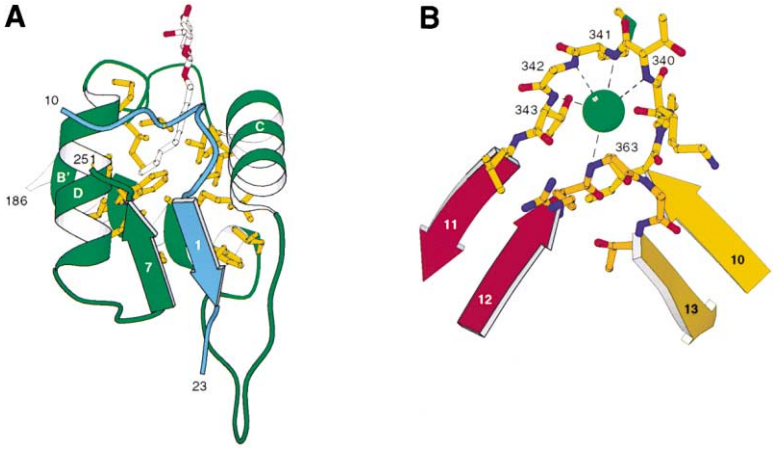

Figure 5. Characteristic Features of the μ1 Molecule

(A) Putative N-myristoyl binding site in domain II framed by a helix-turn-helix motif and a short antiparallel β sheet. The β-octyl glucoside molecule is shown in light gray; hydrophobic side chains contributing to the pocket, in yellow.

(B) Sulfate binding site in domain IV. The sulfate, bound on the upper surface of the μ1 trimer, is coordinated by five main chain amide groups from a β-hairpin insertion into the jelly-roll fold. The sulfate ion is in green; the β-hairpin, in red; the jelly-roll β strands, in yellow.

of density at the center of each ring of six $\mu1_3\sigma3_3$ complexes (Figure 6A). This feature is at approximately the same radial position in the particle as the last well-ordered μ1 residue, Pro 675, and the distance between Pro 675 and the center of the blob is about 16 Å. We therefore propose that the six C-terminal tails of μ1 that project toward a local 6-fold axis in the virion form a small, globular domain. This domain might, for example, resemble the β annulus formed by N-terminal arms of quasi-6-fold related subunits in CCMV (Speir et al., 1995). Cys679, of μ1, would probably take part in the proposed globular structure. Thus, disulfide bonds crosslinking heterohexamers (A. Odegard et al., personal communication) could also contribute to stability of the outer capsid.

Relation of μ1 to Proteins in Other dsRNA Viruses

The folded structure of the μ1 polypeptide chain bears noticeable similarity to those of the VP6 subunits from rotaviruses and the VP7 subunits from orbiviruses (Grimes et al., 1995; Mathieu et al., 2001). All contain central, jelly-roll, β barrel domains, preceded and followed in the sequence by helical elements that form trimeric "pedestals." Moreover, in all three cases, the trimers assemble into a T = 13*l* icosahedral lattice, fenestrated in the case of the orthoreoviruses. The functions and modes of attachment to the underlying structure differ among the various classes of dsRNA viruses (Nibert and Schiff, 2001; Estes, 2001; Roy, 2001). Thus, structurally related proteins occupying similar locations in the virion have acquired divergent functions in the course of evolving distinct patterns of virus-cell interaction.

Role of μ1 in Viral Entry

Like all viruses, reoviruses undergo a programmed series of structural transformations in order to enter a cell. Early steps in this series are formation of the ISVP by proteolytic degradation of σ3 and autolytic cleavage of μ1 at the μ1N/μ1C junction. Receptor binding (facilitated by the projecting conformation of σ1 found in the ISVP) and endocytosis place the particle within a membrane-bound endosome. To advance the infection further and to deposit the core into the cytoplasm, μ1 must disrupt the endosomal membrane. Loss of σ3 and autolytic cleavage prime μ1 for its penetration function.

The structure of $\mu1_3\sigma3_3$ and its interactions in the surface of the ISVP indicate likely steps in the molecular mechanism of penetration. The tight insertion of σ3 between adjacent μ1 subunits in the heterohexamer shows that σ3 removal will indeed destabilize the μ1 trimer and suggests why proteolysis is required to extract σ3. The lattice contacts within the surface of the ISVP, revealed by the fit of the heterohexamer into the cryoEM map, and the inferred interactions of μ1 C-terminal tails, including proposed disulfide bridges, prevent immmediate conformational rearrangement of μ1, once σ3 departs. As we discuss above, the timing of μ1 cleavage is uncertain, relative to the other events in ISVP formation and viral attachment, but the cleavage is clearly required for infectivity of in vitro reconstituted virions. That is, cores can be recoated successfully with uncleavable $\mu1_3\sigma3_3$ containing μ1(Asn42 → Ala), but the reconstituted particles are not infectious (A. Odegard, K.C., and M.N, unpublished). Our structure shows that the cleavage itself is not accompanied by a major conformational change. That is, proteolytic stripping of σ3 and autolytic cleavage of μ1 render the μ1 trimer metastable, but some property of the cellular compartment from which the virus penetrates must catalyze rearrangement to a penetration-active conformation.

What sorts of rearrangements might we picture? Conservation of the μ1N/μ1C cleavage and placement of the myristoyl pocket strongly suggest that release of μ1N from μ1C is an essential part of the penetration process (Figure 7). Myristoyl moieties on proteins generally have membrane-targeting functions, and most or all of the μ1N peptide must dissociate from μ1C to allow the myristoyl chain to insert into a membrane. The tight interaction of μ1N with key structural elements in both the N- and C-terminal parts of μ1C (see, for example, its inclusion with segments of μ1C in a β sheet: Figure 3) further implies that domains I and II (and perhaps also domain III) must unfold in the process of μ1N release. The trigger for these conformational changes may be associated with conditions in the endosome or with the proximity of a lipid bilayer. The only potentially membrane-interactive feature identified so far on the outward-facing surface of μ1 is the anion binding site. If this indeed represents a site for recognition of phospholipid head groups, it is possible that membrane contacts are involved in unleashing μ1 conformational rearrangements.

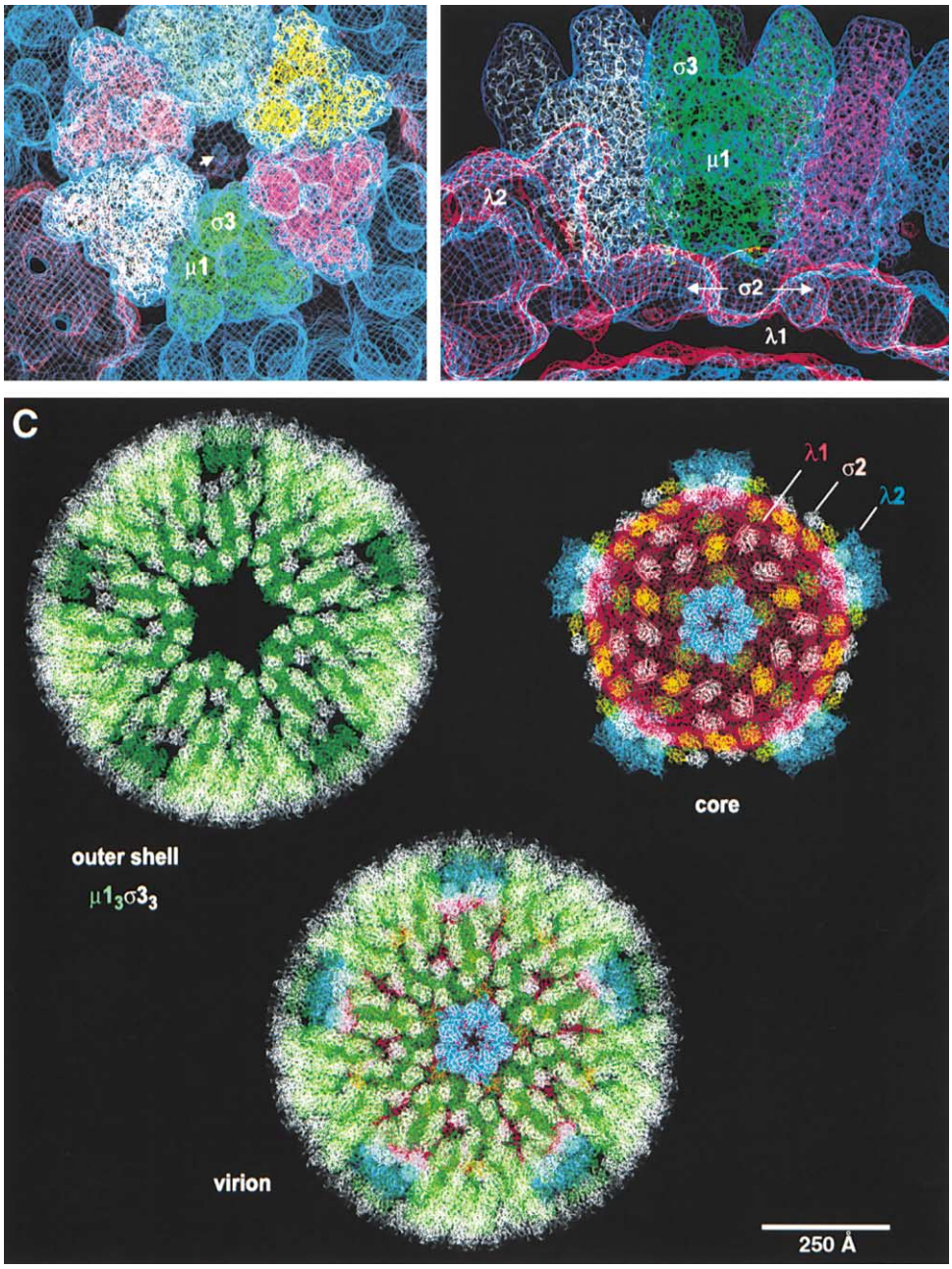

Figure 6. Fit of Atomic Structures into a Cryo-EM Image of the T1L Virion

(A) View from outside the particle. The contours of the EM map of the virion are in blue, with contours for the core also shown in red. Six $\mu1_3\sigma3_3$ complexes were placed in the virion map as shown by the colored models (see Experimental Procedures). The jelly-roll domains IV of $\mu1$ subunits in neighboring trimers contact each other through loops between strands 13 and 14, 15 and 16, and 19 and 20; the central domains II make contact through helices K and through the loops between helices C and D, and E and F; the basal domains I make contact through helices B and through the loops between helix A′ and strand 5. The isolated blob (arrow) in the center of the ring of six $\mu1$ trimers probably represents a clustering of the C-terminal arms from the six neighboring $\mu1$ subunits. The loops of $\mu1$ containing residues 51–62 and (probably) the disordered loop containing residues 72–96 mediate variable contacts with the 150 $\sigma2$ subunits on the underlying surface of the core. (B) Cross-sectional view. A pentameric $\lambda2$ turret is on the left; the $\sigma2$ monomers, bound on the surface of the $\lambda1$ shell, support the $\mu1$ lattice. (C) A synthetic, quasi-atomic model of the reovirus particle. The outer shell of 200 $\mu1_3\sigma3_3$ heterohexamers is represented on the upper left, with $\mu1$ in green and $\sigma3$ in white; the core (Reinisch et al., 2000) is on the upper right, with $\lambda1$ in red, $\lambda2$ in blue, and $\sigma2$ in pink and yellow; the combination of the two models, which includes all icosahedrally ordered proteins in the virion (a total of 100 MDa), is at the bottom.

The structure and its likely rearrangements suggest two different membrane insertion events. One would involve the myristoyl group of $\mu1$N, as described above. The other might involve a more extensive insertion of one or more segments of domains I–III, in a completely refolded state, similar to the events believed to occur when diptheria toxin, colicin Ia, or exotoxin A penetrate endosomal membranes (Gouaux, 1997; Lesieur et al.,

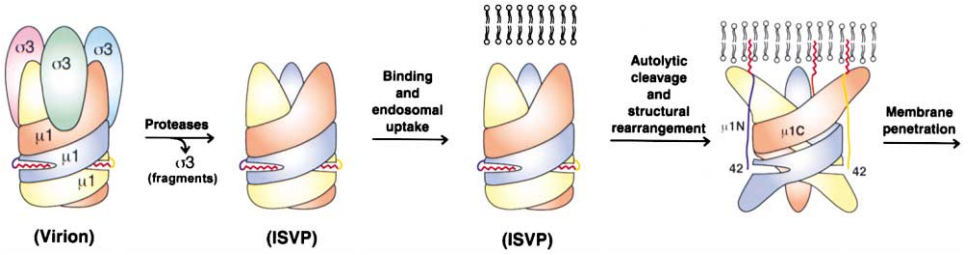

Figure 7. Schematic Model of μ1 Transformations in Reovirus Entry

Proteolytic removal of σ3 (left) prepares the μ1 trimer to undergo a conformational change in the endosome (right). Unfolding of μ1C is suggested by uncoiling of the schematic trimer; the actual rearrangement may be considerably more extensive. Release of μ1N allows the myristoyl group to insert into the membrane. The stage at which autolytic cleavage separates μ1N from μ1C is not yet known.

1997). For the largely helical domains I–III to refold and insert, it is probably essential for the β-jelly-roll domains of a trimer to separate from each other and to move away from the 3-fold axis. Otherwise, domains I–III would have to project around the sides of the jelly-roll trimer, or the entire assembly would have to turn "upside down."

The properties of certain ethanol-resistant mutants of reovirus (Hooper and Fields, 1996b) are consistent with the suggestion just made, that the jelly-roll domains separate during a penetration-inducing conformational change. The mutations, which all map to μ1, also make the particle more thermostable and reduce the capacity of ISVPs to mediate ^{51}Cr release from cells (Hooper and Fields, 1996b). It is therefore likely that they hinder rearrangements in μ1 essential for perforating membranes and for facilitating viral penetration. All of these mutations are in residues on the surface of the μ1 jelly-roll domain. Some face the hydrophilic channel along the 3-fold axis, where they might produce the observed phenotype by stabilizing the trimer itself and preventing the postulated separation of jelly-roll domains. Others lie at positions of contact between adjacent trimers in the ISVP surface, where they might stabilize the T = 13*l* lattice contacts and have a similar effect. The network of μ1 contacts within this surface lattice would be expected to impart marked cooperativity to any μ1 conformational change. Thus, a large number of μ1 trimers would rearrange simultaneously, leading to endosomal membrane disruption or to formation of a "penetration pore."

Further evidence for substantial conformational rearrangements in μ1 during viral penetration comes from recent observations of a correlation between generalized protease sensitivity of μ1C and membrane disruption, as measured by ISVP induced hemolysis and by ISVP-induced leakage of fluorophores from preloaded liposomes (Chandran, 2001; K.C. and M.N., in preparation). When ISVPs are rendered labile by mild warming or by changes in cations, μ1 becomes sensitive to proteolysis; these preparations will then lyse red blood cells or liposomes. Unfolding of μ1 (as monitored by protease accessibility) is evidently required for membrane disruption.

Our description of the μ1 trimer, stripped of σ3 and autolytically cleaved to μ1N and μ1C, as a metastable assembly, immediately suggests an analogy with influenza virus hemagglutinin (HA) and other viral fusion proteins. Once cleaved into HA_1 and HA_2, influenza HA is metastable; proton binding at the acidic pH of the endosome triggers an irreversible conformational rearrangement that induces membrane fusion (Skehel and Wiley, 2000). Proton binding catalyzes the change by lowering the barrier between the metastable "mature" structure and the rearranged, "low-pH" structure.

Exposure of a myristoylated, internal peptide or internal protein is a conserved feature of viral entry in several groups of nonenveloped viruses. Picornavirus maturation includes an autolytic cleavage step, which creates an internal, myristoylated peptide known as VP4 (about 65 residues). VP4 is liberated when association of the virion with its receptor catalyzes an expansion of the virus particle (Racaniello, 2001). VP4 is known to have a role in picornavirus penetration, but the specific mechanism by which it assists transfer of the altered virion or of the viral genome into the cytoplasm is not at present understood. The common features of picornavirus and reovirus biochemistry are striking: an essential, autolytic step generates a sequestered, myristoylated segment that emerges as part of the penetration process. Moreover, in both cases, the cleavage itself may render the native structure metastable, and a defined, biologically significant event (receptor binding in the case of the picornaviruses, an as yet undetermined interaction in the case of the reoviruses) triggers exposure, and presumably membrane targeting, of the myristoylated peptide. Polyomaviruses also contain an internal, myristoylated protein, known as VP2. A mutation that prevents myristoylation also greatly retards early steps in viral entry (Moscufo et al., 1993). Further details of the mechanism by which polyomavirus VP2 emerges and of the way in which it facilitates entry have not yet been uncovered.

The rearrangement of μ1 we have postulated is an example of a "myristoyl switch." Many N-myristoylated proteins are regulated by myristoyl-group exposure or sequestration, which accompanies a conformational change. Calcium binding is the trigger for myristoyl exposure in the case of the neuronal calcium sensor recoverin (Ames et al., 1997; Tanaka et al., 1995), GTP binding, in the case of the ARF small GTPase (Goldberg, 1998). We have not yet identified a trigger for the myristoyl switch in μ1, but candidates include interaction with lipid head groups at the anion binding site and conditions in the lumen of the endosome.

Thus, the structure of the $\mu1_3\sigma3_3$ complex suggests that it carries out the task of inserting a reovirus core across a membrane through major conformational rearrangements and multiple membrane interactions. Pro-

teolytic removal of σ3, in the intestinal lumen or in an endosome, and autolytic cleavage of μ1 prepare this penetration machine, but interactions within the surface lattice of the ISVP hold it in a primed conformation. A triggering event, yet to be determined but perhaps involving contact of the jelly-roll domain with an endosomal membrane and reduction or shuffling of disulfide bonds, causes the helical domains of μ1C to unfold, releasing μ1N, and to refold, probably into a membrane-associated structure. Many copies of μ1N, and of the putatively rearranged μ1C, are probably needed to form a penetration pore or to disrupt the membrane sufficiently for translocation of the reovirus core.

Experimental Procedures

Protein Expression and Purification

$\mu1_3\sigma3_3$ was prepared by coproduction of the T1L μ1 and σ3 proteins in insect cells infected with a recombinant baculovirus carrying the T1L M2 and S4 genes (Chandran et al., 1999). Sf21 cells were grown in Hink's TNM-FH insect medium (JRH) supplemented with 10% (v/v) fetal bovine serum (Sigma), infected at one plaque-forming unit/cell and harvested 70 hr postinfection. The cells were suspended in resuspension buffer (20 mM Tris-HCl [pH 8.5], 2 mM $MgCl_2$, 150 mM KCl, 5 mM DTT, 2 mM benzamidine, 2 μg/ml pepstatin A, 2 μg/ml leupeptin, and 0.2 mg/ml PMSF, supplemented with complete EDTA-free protease inhibitor cocktail [Roche]), 1 ml/5×10^7 cells, and disrupted by sonication. Cell debris was removed by centrifugation (180,000 × g, 2 hr, 4°C); the supernatant was applied to an HP Q-Sepharose column (Amersham Pharmacia Biotech), equilibrated with buffer A (20 mM Tris-HCl [pH 8.5], 2 mM $MgCl_2$, and 5 mM DTT) plus 150 mM NaCl. $\mu1_3\sigma3_3$ was eluted with a linear salt gradient (150–450 mM NaCl in buffer A). The fractions containing $\mu1_3\sigma3_3$ were pooled; 4 M $(NH_4)_2SO_4$, buffered in 20 mM Tris-HCl (pH 8.5), was added dropwise to a final concentration of 0.7 M. The protein was loaded on an HP Phenyl-Sepharose column (Amersham Pharmacia Biotech) equilibrated in buffer A plus 0.7 M $(NH_4)_2SO_4$ and eluted with a linear gradient of 0.7–0 M $(NH_4)_2SO_4$ in buffer A. The protein solution was diluted 1:5 with buffer A and applied to a MonoQ column (Amersham Pharmacia Biotech), equilibrated with buffer A plus 170 mM NaCl, from which $\mu1_3\sigma3_3$ was eluted with a linear salt gradient (170–320 mM NaCl in buffer A). The protein complex was further purified by size exclusion chromatography (Superdex200; Amersham Pharmacia Biotech) in buffer B (20 mM Bicine-HCl (pH 9.0), 2 mM $MgCl_2$, 10 mM DTT, 100 mM NaCl, and 0.02% NaN_3). The final yield was 1.5 mg $\mu1_3\sigma3_3$ per liter of Sf21 cells. The pure protein was concentrated to 3 mg/ml by ultrafiltration (Amicon Centricon, Millipore) and stored at −80°C.

The mass of the complex was determined by sedimentation equilibrium analytical ultracentrifugation (Optima XL-A analytical ultracentrifuge, Beckman Coulter) at room temperature with three different protein starting concentrations (0.1, 0.2, and 0.3 mg/ml). The curves of absorbance versus radius fit the distribution for a molecular mass of 350 kDa, corresponding to a $\mu1_3\sigma3_3$ heterohexamer.

SeMet labeled $\mu1_3\sigma3_3$ was prepared in insect cells by adapting a protocol originally designed for secreted proteins (Bellizzi et al., 1999; Chen and Bahl, 1991). Briefly, Sf21 cells were grown and infected as described above, but 8 hr postinfection, the growth medium was exchanged for depletion medium (Grace's medium without L-methionine [Life Technologies] supplemented with 5% [v/v] dialyzed fetal bovine serum [Sigma]). Seleno-L-methionine (Sigma) was added to a final concentration of 50 μg/ml at 17 hr postinfection, prior to observation of significant expression levels of $\mu1_3\sigma3_3$ by immunoblot with a $\mu1_3\sigma3_3$-specific polyclonal antibody (Millbrook Breeding Labs). Cells were harvested 70 hr postinfection; the protein was purified as described using degassed buffers with the addition of 10 mM DTT. Incorporation of SeMet was determined by electrospray mass spectrometry and amino acid analysis to be 100% for both μ1 and σ3.

For the Hg derivative of $\mu1_3\sigma3_3$, cysteine was substituted for the nonconserved σ3 residue Ala104, seen from a fit of the σ3 structure to a three-dimensional EM reconstruction of the T1L virion to be on the surface of $\mu1_3\sigma3_3$ (Olland et al., 2001). The pFastbacDUAL vector (Life Technologies) containing the T1L M2 and S4 genes, pFbD-M2L-S4L (Chandran et al., 1999), was digested with KpnI (New England Biolabs). The fragment carrying the S4 gene was cloned into pBluescriptII SK(+) (Stratagene) and site-directed mutagenesis performed by the QuikChange protocol (Stratagene). The mutated S4 genes were sequenced and cloned back into pFbD-M2L-S4L. A recombinant baculovirus was generated with the Bac-to-Bac Baculovirus Expression System (Life Technologies). The $\mu1_3\sigma3_3$-A104C (S4) variant was purified in the presence of 10 mM DTT.

Crystallization and Data Collection

Crystals of $\mu1_3\sigma3_3$ were grown by vapor diffusion at room temperature in hanging drops with 1 μl protein sample, 1 μl reservoir solution (100 mM Pipes/NaOH [pH 7.0], 0.5 M $(NH_4)_2SO_4$, and 10 mM DTT) plus 0.07% (w/v) n-octyl-β-D-glucopyranoside (Anatrace). Crystals, in space group I222 (a = 182.29 Å, b = 184.94 Å, c = 284.32 Å), one heterohexamer per asymmetric unit, grew as very thin plates in 1–2 days to 350 × 120 × 10 μm. An inherent growth defect rendered only one out of about 20 crystals useful for structure determination. Crystals were stabilized in 100 mM Pipes-NaOH (pH 7.0), 0.8 M ammonium sulfate, 0.07% β-octyl glucoside (stabilizing buffer) at room temperature overnight, transferred in 5% steps to 25% glycerol in the stabilizing buffer, and flash-frozen in liquid nitrogen. For the Hg derivative, crystals of the $\mu1_3\sigma3_3$-A104C (S4) variant were soaked overnight in 20 μM methyl-mercury nitrate at 14°C. Diffraction data were recorded at the National Synchrotron Light Source (Brookhaven National Laboratory, NY) beamline X25 using the Brandeis 4-element CCD detector. Intensities were integrated and scaled using DENZO and SCALEPACK (Otwinowski and Minor, 1993).

Structure Determination and Refinement

The $\mu1_3\sigma3_3$ structure was determined by MIR with anomalous scattering and 3-fold NCS averaging. Native and derivative data sets were scaled using CCP4 programs (Collaborative Computational Project N, 1994). Starting heavy-atom positions for the Hg derivative were determined by inspection of isomorphous difference Patterson maps (15–5 Å); additional sites, a total of 12, were found from isomorphous difference Fourier maps. Heavy atom parameters were refined (15–3.5 Å) with MLPHARE (Collaborative Computational Project N, 1994); inclusion of anomalous occupancies allowed determination of the correct hand. The 3-fold NCS operator, nearly parallel to the z axis ($\theta = 3.5°$) as shown by a self-rotation function, was determined from the position of the 12 Hg sites. Phases were improved by density modification, solvent flattening, histogram matching, and 3-fold NCS averaging (density correlation: 86.8%) with DM (Collaborative Computational Project N, 1994). The improved phases were used to locate three additional Hg sites, and 93 Se sites (out of 111 methionines in the asymmetric unit) were found in the SeMet derivative from a 3-fold averaged isomorphous difference Fourier map. All 108 heavy atom positions and their anomalous occupancies were refined in MLPHARE, and the NCS operator was redetermined. Phases were improved in DM and extended to a resolution of 2.8 Å. A μ1-σ3 protomer was built with the program O (Jones et al., 1991) into the experimental electron density map. The model was refined with CNS (Brunger et al., 1998) by simulated annealing and positional refinement, initially with strict NCS constraints and later with tight NCS restraints, using 5% of the data for cross validation. After several rounds of refinement and model building, waters were built automatically using CNS. We used PROCHECK (Laskowski et al., 1993) to analyze the stereochemistry of the final model; 86.5% of the backbone dihedral angles were in the most favorable region, 13.2% in the favorable region, and 0.2% in the unfavorable region of a Ramachandran plot. The rms differences to the reference set are 0.041 Å and 0.034 Å for the three σ3 molecules and 0.028 Å and 0.029 Å for the three μ1 molecules, respectively.

Fit of the $\mu1_3\sigma3_3$ Model into the Virion Image Reconstruction from Electron Microscopy

The $\mu1_3\sigma3_3$ structure was positioned visually into the image reconstruction of a T1L virion at 18 Å resolution at the symmetry-indepen-

dent positions in the T13*I* lattice. Crystallographic structure factors and phases of the positioned model were determined and used to calculate an electron density map at 18 Å using CCP4 programs (Collaborative Computational Project N, 1994). Real-space maximization of the correlation coefficient (within a protein mask derived from the crystal structure) between the virion map and the calculated $\mu1_3\sigma3_3$ electron density was conducted using RAVE (Kleywegt and Jones, 1999). Correlation coefficients of 0.80 to 0.83 were observed for the different symmetry positions in the T13*I* lattice.

Preparation of Figures

Figures were prepared with the programs MOLSCRIPT (Kraulis, 1991), ALSCRIPT (Barton, 1993), GRASP (Nicholls et al., 1991), and O (Jones et al., 1991).

Acknowledgments

We thank Sophia Rits-Volloch for expression of the SeMet-labeled protein; David King at HHMI, Berkeley, and John Rush at the Biopolymers Facility, Harvard Medical School, for mass spectrometry; L. Berman, M. Becker, and H. Lewis at beamline X25 at NSLS BNL and W. Schildkamp, R. Pahl, and the staff of beamline 14-C at BioCARS (APS) for assistance with data collection; and members of the Harrison and Wiley research groups, especially Andrea Carfí and Jens Hennecke, for discussions. This work has been supported by grants from the NIH (CA-13202 to S.C.H., AI-46440 to M.L.N., and GM-33050 to T.S.B.). S.L. was supported by a postdoctoral BASF research fellowship of the Studienstiftung des deutschen Volkes and is now an HHMI associate. K.C. was supported by a pre-doctoral fellowship from the Howard Hughes Medical Institute. S.C.H. is an investigator in the Howard Hughes Medical Institute.

Received August 8, 2001; revised December 10, 2001.

References

Ames, J.B., Ishima, R., Tanaka, T., Gordon, J.I., Stryer, L., and Ikura, M. (1997). Molecular mechanics of calcium-myristoyl switches. Nature *389*, 198–202.

Barton, G.J. (1993). ALSCRIPT: a tool to format multiple sequence alignments. Protein Eng. *6*, 37–40.

Bellizzi, J.J., Widom, J., Kemp, C.W., and Clardy, J. (1999). Producing selenomethionine-labeled proteins with a baculovirus expression vector system. Struct. Fold. Des. *7*, R263–267.

Borsa, J., Morash, B.D., Sargent, M.D., Copps, T.P., Lievaart, P.A., and Szekely, J.G. (1979). Two modes of entry of reovirus particles into L cells. J. Gen. Virol. *45*, 161–170.

Borsa, J., Sargent, M.D., Lievaart, P.A., and Copps, T.P. (1981). Reovirus: evidence for a second step in the intracellular uncoating and transcriptase activation process. Virology *111*, 191–200.

Bossemeyer, D. (1994). The glycine-rich sequence of protein kinases: a multifunctional element. Trends Biochem. Sci. *19*, 201–205.

Brunger, A.T., Adams, P.D., Clore, G.M., DeLano, W.L., Gros, P., Grosse-Kunstleve, R.W., Jiang, J.S., Kuszewski, J., Nilges, M., Pannu, N.S., et al. (1998). Crystallography & NMR system: a new software suite for macromolecular structure determination. Acta Crystallogr. D Biol. Crystallogr. *54*, 905–921.

Chandran, K. (2001). PhD Thesis, University of Wisconsin, Madison.

Chandran, K., and Nibert, M.L. (1998). Protease cleavage of reovirus capsid protein $\mu1/\mu1C$ is blocked by alkyl sulfate detergents, yielding a new type of infectious subvirion particle. J. Virol. *72*, 467–475.

Chandran, K., Walker, S.B., Chen, Y., Contreras, C.M., Schiff, L.A., Baker, T.S., and Nibert, M.L. (1999). In vitro recoating of reovirus cores with baculovirus-expressed outer-capsid proteins $\mu1$ and $\sigma3$. J. Virol. *73*, 3941–3950.

Chang, C.T., and Zweerink, H.J. (1971). Fate of parental reovirus in infected cell. Virology *46*, 544–555.

Chen, W.Y., and Bahl, O.P. (1991). Selenomethionyl analog of recombinant human choriogonadotropin. J. Biol. Chem. *266*, 9355–9358.

Collaborative Computational Project N. (1994). The CCP4 suite: programs for protein crystallography. Acta Crystallogr. *D50*, 760–763.

Dryden, K.A., Wang, G., Yeager, M., Nibert, M.L., Coombs, K.M., Furlong, D.B., Fields, B.N., and Baker, T.S. (1993). Early steps in reovirus infection are associated with dramatic changes in supramolecular structure and protein conformation: analysis of virions and subviral particles by cryoelectron microscopy and image reconstruction. J. Cell Biol. *122*, 1023–1041.

Estes, M. (2001). Reoviruses and their replication. In Fields Virology, D.M. Knipe and P.M. Howley, eds. (Philadelphia: Lippincott Williams and Wilkins), pp. 1747–1785.

Fields, B.N., Raine, C.S., and Baum, S.G. (1971). Temperature-sensitive mutants of reovirus type 3: defects in viral maturation as studied by immunofluorescence and electron microscopy. Virology *43*, 569–578.

Furlong, D.B., Nibert, M.L., and Fields, B.N. (1988). $\sigma1$ protein of mammalian reoviruses extends from the surfaces of viral particles. J. Virol. *62*, 246–256.

Goldberg, J. (1998). Structural basis for activation of ARF GTPase: mechanisms of guanine nucleotide exchange and GTP-myristoyl switching. Cell *95*, 237–248.

Gouaux, E. (1997). Channel-forming toxins: tales of transformation. Curr. Opin. Struct. Biol. *7*, 566–573.

Grimes, J., Basak, A.K., Roy, P., and Stuart, D. (1995). The crystal structure of bluetongue virus VP7. Nature *373*, 167–170.

Harrison, S.C. (2001). Virus structure. In Fields Virology, D.M. Knipe and P.M. Howley, eds. (Philadelphia: Lippincott Williams and Wilkins), pp. 53–85.

Holm, L., and Sander, C. (1993). Protein structure comparison by alignment of distance matrices. J. Mol. Biol. *233*, 123–138.

Hooper, J.W., and Fields, B.N. (1996a). Monoclonal antibodies to reovirus $\sigma1$ and $\mu1$ proteins inhibit chromium release from mouse L cells. J. Virol. *70*, 672–677.

Hooper, J.W., and Fields, B.N. (1996b). Role of the $\mu1$ protein in reovirus stability and capacity to cause chromium release from host cells. J. Virol. *70*, 459–467.

Huismans, H., and Joklik, W.K. (1976). Reovirus-coded polypeptides in infected cells: isolation of two native monomeric polypeptides with affinity for single-stranded and double-stranded RNA, respectively. Virology *70*, 411–424.

Imani, F., and Jacobs, B.L. (1988). Inhibitory activity for the interferon-induced protein kinase is associated with the reovirus serotype 1 $\sigma3$ protein. Proc. Natl. Acad. Sci. USA *85*, 7887–7891.

Jayasuriya, A.K., Nibert, M.L., and Fields, B.N. (1988). Complete nucleotide sequence of the M2 gene segment of reovirus type 3 dearing and analysis of its protein product $\mu1$. Virology *163*, 591–602.

Jones, T.A., Zou, J.Y., Cowan, S.W., and Kjeldgaard. (1991). Improved methods for binding protein models in electron density maps and the location of errors in these models. Acta Crystallogr. A *47*, 110–119.

Kabsch, W., and Sander, C. (1983). Dictionary of protein secondary structure: pattern recognition of hydrogen-bonded and geometrical features. Biopolymers *22*, 2577–2637.

Kleywegt, G.J., and Jones, T.A. (1999). Software for handling macromolecular envelopes. Acta Crystallogr. D Biol. Crystallogr. *55*, 941–944.

Kraulis, P.J. (1991). MOLSCRIPT: a program to produce both detailed and schematic plots of protein structures. J. Appl. Crystallogr. *24*, 946–950.

Laskowski, R.A., Moss, D.S., and Thornton, J.M. (1993). Main-chain bond lengths and bond angles in protein structures. J. Mol. Biol. *231*, 1049–1067.

Lee, P.W., Hayes, E.C., and Joklik, W.K. (1981). Protein $\sigma1$ is the reovirus cell attachment protein. Virology *108*, 156–163.

Lesieur, C., Vecsey-Semjen, B., Abrami, L., Fivaz, M., and Gisou van der Goot, F. (1997). Membrane insertion: the strategies of toxins (review). Mol. Membr. Biol. *14*, 45–64.

Lucia-Jandris, P., Hooper, J.W., and Fields, B.N. (1993). Reovirus M2 gene is associated with chromium release from mouse L cells. J. Virol. *67*, 5339–5345.

Mathieu, M., Petitpas, I., Navaza, J., Lepault, J., Kohli, E., Pothier, P., Prasad, B.V., Cohen, J., and Rey, F.A. (2001). Atomic structure of the major capsid protein of rotavirus: implications for the architecture of the virion. EMBO J. *20*, 1485–1497.

Moscufo, N., Yafal, A.G., Rogove, A., Hogle, J.M., and Chow, M. (1993). A mutation in VP4 defines a new step in the late stages of cell entry by poliovirus. J. Virol. *67*, 5075–5078.

Nibert, M.L., and Fields, B.N. (1992). A carboxy-terminal fragment of protein μ1/μ1C is present in infectious subvirion particles of mammalian reoviruses and is proposed to have a role in penetration. J. Virol. *66*, 6408–6418.

Nibert, M.L., Schiff, L.A., and Fields, B.N. (1991). Mammalian reoviruses contain a myristoylated structural protein. J. Virol. *65*, 1960–1967.

Nibert, M.L., and Schiff, L.A. (2001). Reoviruses and their replication. In Fields Virology, D.M. Knipe and

P.M. Howley, eds. (Philadelphia: Lippincott Williams and Wilkins), pp. 1679–1728.

Nicholls, A., Sharp, K.A., and Honig, B. (1991). Protein folding and association: insights from the interfacial and thermodynamic properties of hydrocarbons. Proteins *11*, 281–296.

Olland, A.M., Jane-Valbuena, J., Schiff, L.A., Nibert, M.L., and Harrison, S.C. (2001). Structure of the reovirus outer capsid and dsRNA-binding protein σ3 at 1.8 A resolution. EMBO J. *20*, 979–989.

Otwinowski, Z., and Minor, W. (1993). Processing of x-ray diffraction data collected in oscillation mode. Methods Enzymol. *276*, 307–326.

Racaniello, V.R. (2001). Picornaviridae: the viruses and their replication. In Fields Virology, D.M. Knipe and P.M. Howley, eds. (Philadelphia: Lippincott Williams and Wilkins), pp. 685–722.

Reinisch, K.M., Nibert, M.L., and Harrison, S.C. (2000). Structure of the reovirus core at 3.6 Å resolution. Nature *404*, 960–967.

Roy, P. (2001). Orbiviruses. In Fields Virology, D.M. Knipe and P.M. Howley, eds. (Philadelphia: Lippincott Williams and Wilkins), pp. 1835–1869.

Saraste, M., Sibbald, P.R., and Wittinghofer, A. (1990). The P-loop—a common motif in ATP- and GTP-binding proteins. Trends Biochem. Sci. *15*, 430–434.

Schiff, L.A., Nibert, M.L., Co, M.S., Brown, E.G., and Fields, B.N. (1988). Distinct binding sites for zinc and double-stranded RNA in the reovirus outer capsid protein σ*3.* Mol. Cell. Biol. *8*, 273–283.

Sharpe, A.H., and Fields, B.N. (1982). Reovirus inhibition of cellular RNA and protein synthesis: role of the S4 gene. Virology *122*, 381–391.

Shatkin, A.J., and LaFiandra, A.J. (1972). Transcription by infectious subviral particles of reovirus. J. Virol. *10*, 698–706.

Shing, M., and Coombs, K.M. (1996). Assembly of the reovirus outer capsid requires μ 1/σ3 interactions which are prevented by misfolded σ3 protein in temperature-sensitive mutant tsG453. Virus Res. *46*, 19–29.

Silverstein, S.C., Schonberg, M., Levin, D.H., and Acs, G. (1970). The reovirus replicative cycle: conservation of parental RNA and protein. Proc. Natl. Acad. Sci. USA *67*, 275–281.

Skehel, J.J., and Wiley, D.C. (2000). Receptor binding and membrane fusion in virus entry: the influenza hemagglutinin. Annu. Rev. Biochem. *69*, 531–569.

Speir, J.A., Munshi, S., Wang, G., Baker, T.S., and Johnson, J.E. (1995). Structures of the native and swollen forms of cowpea chlorotic mottle virus determined by X-ray crystallography and cryo-electron microscopy. Structure *3*, 63–78.

Tanaka, T., Ames, J.B., Harvey, T.S., Stryer, L., and Ikura, M. (1995). Sequestration of the membrane-targeting myristoyl group of recoverin in the calcium-free state. Nature *376*, 444–447.

Tillotson, L., and Shatkin, A.J. (1992). Reovirus polypeptide σ3 and N-terminal myristoylation of polypeptide μ1 are required for site-specific cleavage to μ1C in transfected cells. J. Virol. *66*, 2180–2186.

Tosteson, M.T., Nibert, M.L., and Fields, B.N. (1993). Ion channels induced in lipid bilayers by subvirion particles of the nonenveloped mammalian reoviruses. Proc. Natl. Acad. Sci. USA *90*, 10549–10552.

Wiener, J.R., and Joklik, W.K. (1988). Evolution of reovirus genes: a comparison of serotype *1*, 2, and 3 M2 genome segments, which encode the major structural capsid protein μ1C. Virology *163*, 603–613.

Zweerink, H.J., and Joklik, W.K. (1970). Studies on the intracellular synthesis of reovirus-specified proteins. Virology *41*, 501–518.

Accession Numbers

The coordinates have been submitted to the Protein Data Bank with accession number 1JMU.